LEADING CFD MODELS FOR INNOVATIVE NUCLEAR APPLICATIONS AT CRS4

M. Profir, L. Massidda, V. Moreau

CRS4, Science and Technology Park Polaris - Pula (CA), Italy
E-mail: manuela@crs4.it, lucam@crs4.it, moreau@crs4.it

ABSTRACT

In the last 15 years, CRS4 has developed a consolidated experience in CFD simulations in the field of innovative nuclear system. The complexity of the applications has progressively increased during these years and we present three of the most recent ones.
The first application regards the construction of a CFD model of the entire primary coolant loop of MYRRHA, the future Belgian multi-purpose Lead-Bismuth Eutectic (LBE) cooled nuclear reactor, built in the framework of the FP7 SEARCH project. The second application regards the control rod insertion dynamics in the MYRRHA framework, for use in the FP7 MAXSIMA project. The third application concerns the conception of liquid Lead spallation target for the European Spallation Source (ESS), developed during the FP7 THINS project.
The model of the MYRRHA primary coolant loop combines a free-surface flow and a thermal flow, driven by hydraulic pumps. Heat is provided by the reacting nuclear core and removed by heat exchangers and thermal irradiation from the containment vessel. The conjugate heat exchange with the main internal structures is also taken into account. Being a pool reactor, the coolant is in contact with the cover gas. The contact is established at different levels in relation to the pressure drop between the different fluid volumes, essentially between the hot and the cold plenum.
The model of the MYRRHA control rod requires the use of moving meshes in the numerical CFD simulation and a good control of the topological deformations that could lead to important numerical errors. Mesh morphing and re-meshing techniques are employed in the transient analysis of the buoyancy driven control rod system. Full-scale CFD simulations of the control rod displacement in its guide tube are presented. The buoyancy acts as the driving force and the control rod is stopped by a dedicated spring. The model has thus a two-way dynamical coupling.
The model for the ESS requires the analysis of a free surface beam target subject to a pulsed beam deposition. The slow transients of the free surface evolution and the fast transients due to shock wave propagation inside the liquid target are simulated by means of a dedicated code based on the Smoothed Particle Hydrodynamic method implemented on a GPU architecture in order to dramatically increase the performance.

INTRODUCTION

In a global overview of the MYRRHA [1] primary coolant loop, the cold Lead Bismuth Eutectic (LBE) is pushed by the primary pumps (PP) into the core. Here it is heated and then flows into the heat exchangers (HX) where it is cooled down before returning to the pumps. The LBE lays in a pool with two clearly separated free surfaces, one of them possibly separated in two. The level between the free surfaces depends essentially on the pressure drop through the core and on the LBE global inventory. In this context, in the framework of the FP7 SEARCH project, our goal is to study the fuel dispersion in the coolant, due to the loss of integrity of some Fuel Assembly (FA) pins, spanning from one single pin to a partial core melt. The loss of integrity of the fuel pins can be provoked by a variation of the operating conditions, be it local or global. It also can modify the hydraulic characteristics of the FA. For these reasons, we need to be able to act consistently and timely on the operating conditions and we also need to be able to intervene on a single FA basis.

The COMPLOT (COMPonent LOop Testing) is an experimental facility under development at SCK-CEN that will be used to support the MYRRHA reactor design. It will be employed for thermal-hydraulic experiments aimed to test and qualify, among other components, a buoyancy driven safety/control rods (SR/CR) system, as key components for the safe operation in MYRRHA. In the framework of the FP7 MAXSIMA project, we are performing CFD simulations of the full-scale test sections that host the Safety Rod and Control Rod, with all the flow paths included in. We reproduce the CR mechanical movement under buoyancy influence, using moving meshes techniques.

The analysis of fast transients in liquids and of extreme deformations of the free surface such as in splashing phenomena require dedicated tools for the numerical analysis. The Smoothed Particle Hydrodynamic (SPH) is a Lagrangian meshless method, which models the continuum as a set of mutually interacting particles that describe realistically and with good accuracy the motion of fluids, in particular when free surface conditions are present, without any restriction on the density ratio. The fluid is treated as compressible and in our implementation this allows to simulate realistically the formation and propagation of acoustic pressure waves due to the interaction with a beam. The SPH approach is well suited for massively parallel architectures like GPU machines. In the framework of the THINS project, the SPH code Armando, developed at CRS4 in cooperation with CERN, has been ported on GPU architecture and applied to the simulation of a liquid metal free surface target that has been recently proposed for the Eu ropean Spallation Source (ESS) project.

MYRRHA PRIMARY COOLANT LOOP MODEL

In order to characterize the fuel dispersion in the primary coolant we need to obtain a good description of the LBE flow pattern and temperature, as a prerequisite for a sensate convective transport of passive species. Since we want to be able to simulate events such as the loss of a pump or the loss of integrity and dispersion of the fuel of a FA, we are modeling the entire reactor, using mainly the commercial CFD code Star-ccm+ [2]. The detailed description of the current 3D simulation of MYRHHA primary coolant loop is available in [3].

Considerations on the required physics

As the LBE free surface level is a variable feature of the model, we need to be able to let it evolve according to the physics. The multi-phase flow approach is the most suitable one in this sense. As we do not expect neither want the cover gas to mix with the LBE, the Volume of Fluid (VOF) method is better suited, avoiding additional momentum and energy equations. The LBE is clearly incompressible for our purpose, and we do not claim to capture the cover gas dynamics correctly. So, for simplicity, we consider an incompressible cover gas. We are strongly concerned with a possible thermal stratification of the flow, so we must have a temperature dependence of the LBE density. All the necessary physical properties of the LBE are publicly available in the hanbook [4].

Given the complexity of some of the components, porous media have been used in two cases: for the HXs, as the discretization of hundreds of pipes in the centimeter range is too expensive in terms of computational costs and for the above core grids, thin complex structures enforcing the flow vertically.

As we are investigating a thermal cycle, the flow equation is coupled with an energy equation. To take into account the nuclear core and the cold secondary coolant in the HX, an appropriate source term is defined in the energy equation. The coupling is both way because we expect a buoyant flow and we need to take into account temperature dependence of density to capture any thermal stratification.

The structural part plays its part in the thermal inertia of the system. Thermal stratification may be strongly influenced by the heat flow through the structural parts. At steady state, the flow is controlled by an equilibrium between the pump thrust and the hydraulic resistance of the system. While both effects should be resulting from the contact with the structure, they are effectively mainly modeled as body forces.

In Star-ccm+, simulations using VOF must be performed in transient mode. The time required to approach the global thermal equilibrium is quite long, at least several minutes. The flow is clearly turbulent, even if we expect a quiet free surface, hence we run the simulation based on URANS equations using realizable $k-\varepsilon$ turbulence model.

Geometrical, physical and numerical settings

In order to give an idea about the geometry of the computational model we illustrate in Figure 1 the solid support structure which matches the fluid separation in regions. The geometrical parts will be transformed in computational regions. Splitting in regions is needed as the specificity of the physics used is strongly region based. The more regions we use, the more flexibility we have in operate on the physics at a local scale. The cost is an increased complexity of the model and the burden to deal with a large number of interfaces. However, when smartly localized, the interfaces are optimal positions to measure fluxes.

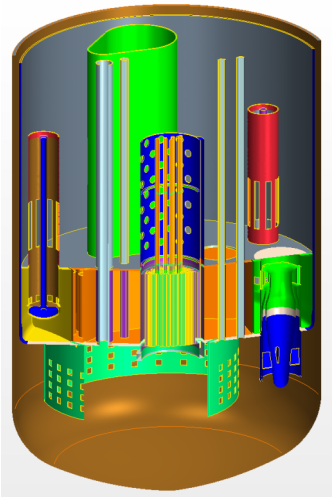

Figure 1. Strucural part of the numerical model

Heat eXchangers (HX). The HX modeling is based on the local application of global considerations. The HX heat source is based on a characteristic time τ and a reference temperature:

$$S = \rho C_p (T_0 - T)/\tau \tag{1}$$

Initially, a quite aggressive term is modeled to get a return to target temperature $T_0 = 270°C$ in a relatively short characteristic time $\tau = 0.7s$. While approaching the thermal equilibrium, we relax the characteristic time and bring the target temperature close to the secondary coolant one: $T_0 = 210°C$, $\tau = 6.6s$.

The HX flow resistance must be consistent with the two phases, with the medium anisotropy and with the turbulent quadratic behavior. The distributed resistance force has the form: $R = -(A + B|v|)v$, decomposed in vertical (small) and planar (large) components. The vertical resistance was retrieved from SCK-CEN analysis and was set in the inertial (quadratic) coefficient B. The transverse loss resulted beyond the SCK-CEN analysis, hence we set the viscous coefficient A dependent on the horizontal velocity modulus only.

Nuclear core. The fuel assemblies are given a flow resistance quadratic in velocity such that the required pressure drop through the core is imposed at nominal flow rate. The energy source is axial-symmetrical with a maximum at the centre and about one half at the border FAs.

Cover gas. The cover gas is out of scope but needs to be carefully handled. Counter-measures must be taken to keep even small volume fractions of the cover gas out of the LBE domain. This is done by setting a sink term of the cover gas phase operating mainly on the free surface, proportional to the product of the mass fractions divided by a characteristic time. The global effect is proportional to the interface width, and thus decreases with the mesh size. The term also very efficiently removes unphysical traces of cover gas in the LBE having the same characteristic time. These traces are difficult to avoid, mainly at flow re-entrance due to solid obstacles. For open flows they are evacuated in outlet, but for a closed loop with cycles, there is a risk of accumulation with an unphysical added buoyancy effect.

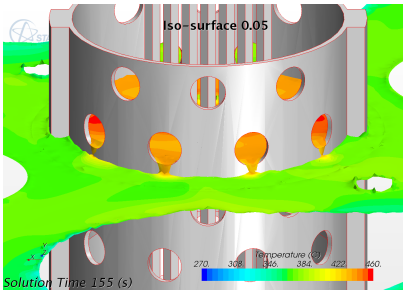

Figure 2. Free surface coloured by temperature around the core barrel

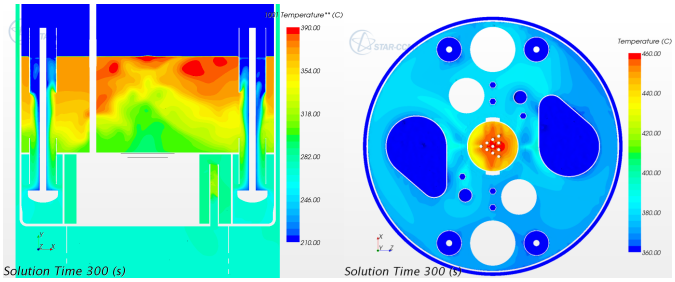

Figure 3. Temperature profile through two HXs (left). Free surface temperature (right)

For the real density ratio (10,000) the VOF algorithm is unstable: to overcome this issue, cover gas density is artificially increased by one order and set independent of temperature. Last but not least, there is a physical inconsistency in making a transient simulation of a buoyant flow in a closed domain. The temperature dependence of the density implies that the mass conservation does not induce a volume conservation. Additionally, the user surface sharpening algorithm just described is not conservative. We are therefore forced to open the computational domain. There is no current boundary condition allowing both inflow and outflow depending on the moment. So, we make what is necessary to be sure that an inflow condition is always required. For this, we create a small outlet region on top of the computational domain, connected to the cover gas region. We put a stagnation inlet boundary at the top of this region and we set a consistent sink term of the cover gas volume fraction. In this way the inflow is ensured even when the LBE volume is increasing due to thermal dilatation.

Route to nominal conditions

Only fluid domain. The first full model did not contemplate the structural part neither the conjugate heat transfer. The flow has been brought at cold plenum temperature to about nominal condition. It takes a few tens of second to get approximately the required flow rates. The filling of the open parts, In Vessel Fuel Handling (IVFH), external ring and various penetrations, where the free surface must rise a couple of meters, is taking some time. Adjustments were made from time to time to the force applied at the pump level. At this point, full thermal power is set inside the core. The HX is set to aggressively bring back the outlet temperature at cold plenum value. It takes about three minutes to reach 85% of the core power in the HX, the remnant part being used to heat the hot plenum. The simulation was restarted with some adjustment of the PP power, the mass flows perturbation being absorbed in about 30s. At a much later stage, when the HX heat sink target temperature has been relaxed, the HX inlet and outlet temperatures become almost constant (340 C, resp. 270 C). The HX power is very close to the nominal 100 MW. Consistently with the mass flows, the free surface has reached its nominal position (its position with respect to the core barrel is shown in Figure 2). It is clear that a small change in the free surface level, due to inclusion or withdrawal of material in the LBE plenum can greatly change the surface temperature profile.

Fluid and solid. The model now takes into account the structures and the heat transfer, following a legitimate suspicion that the temperature in the various fluid upper parts of the cold plenum are in fact hot due to this conjugate heat transfer. The interstitial outer LBE ring temperature is strongly controlled by the balance between the external thermal irradiation and the internal conductive heat flux. It is also possible that the hot plenum thermal stratification is modified. The inclusion of the structural part produces a long time perturbation of the flow field temperature while the flow rates keep unperturbed. This can be explained by the necessity to heat the structural part, initialized at cold plenum temperature, as the thermal inertia of the structural part is not negligible. The HX inlet temperature is not expected to reach the former level as some energy is lost by thermal radiation and also because some structure will keep warming for a long time. Depending on the structure width, the characteristic time for thermal equilibrium is about 15 minutes for the core vessel and more than an hour for the main vessel. Only a partial equilibrium can be reached within the simulation.

Nominal flow. The flow rates at the end of the 300 s simulation are almost stationary, as well as the core and HX temperatures. Some stagnant regions in the cold plenum will continue to get warmer for a very large time, but we do not expect a remarkable influence on the main flow pattern. The temperature in the fluid, retrieved on two vertical profiles across the core, showed that the core barrel structure induces a strong asymmetry of the flow. The temperature profile in the hot plenum and through two HXs illustrated in Figure 3 shows a neat vertical thermal stratification in the plenum and a consistent radial thermal gradient in the HXs.

Flow stability. The model has been further run inserting a swirling component in the PP outflow, allowing to get closer to the global thermal equilibrium. By looking at the temperature profile in Figure 3, one can wonder whether this profile is still evolving and how fast it evolves. The animations drawn from the simulation show that there are still some small changes, mainly at the top of the HX and in the peripheral zone of the free surface but they show a good general stability. The velocity field in Figure 4 shows a perfectly stable profile in the hot plenum and a not so stable profile in the cold plenum with changes in the right PP outflow and a shift of the rising plume towards the core.

Passive scalars: residence time and junk emission

With the model in a reasonably steady state condition, two additional features of the primary loop are investigated, namely the residence time and the debris dispersion characteristics.

The nominal operation is not fully stationary but it is quite close to. So, a relatively long pseudo-transient time evolution of a passive scalar can be done on a frozen flow with a not so degraded accuracy. Since the mean residence time between two passages through the core is about 400 s, we performed a frozen

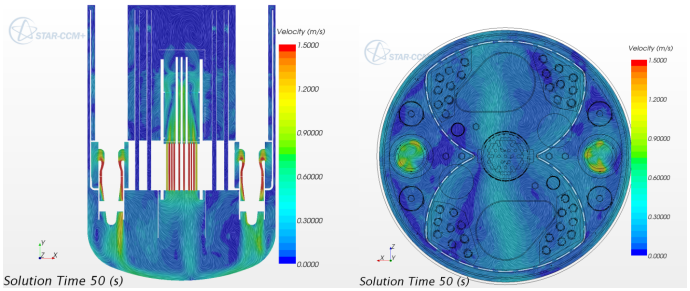

Figure 4. Velocity field at 50 s. Vertical profile (left). Horizontal profile in the cold plenum (right)

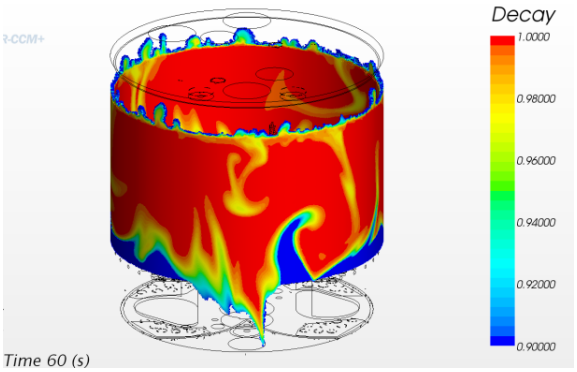

Figure 5. Evolution of the LBE volume initially in the cold plenum annulus

fields simulation for 1200 s in which we followed two different scalars: i) the characteristic residence time from the last passage in the core and ii) a constant junk emission from a central FA.

It is important for corrosion issues to locate all the effective flow stagnation regions where the LBE could be too much depleted of its oxygen content. The characteristic time for an excessive depletion seems to be between several hours and a few days. These are not accessible within a transient simulation, however a partial answer can be given.

Numerically, the residence time is a passive scalar with a source term equal to the density (for the porosity in porous regions) and initialized at zero. In our case, and as we have a closed loop, the residence time is reset to zero while passing through the core. The simulation reveals some critical spots in the vertical penetrations and in the In Vessel Flue Storage (IVFS), but surprisingly much less in the cold plenum annulus.

Some virtual junk is emitted from a central FA and eliminated when re-entering the core. The distribution on a planar section shows that while the junk enters the cold plenum mainly from the right PP, the junk concentration is very homogeneous when re-entering the core. In conformity with the residence time, the junk in not entering the vertical penetrations, but is somehow penetrating into the cold plenum annulus.

To get a better insight on the passive scalars dispersion, we have run an additional 60 s transient RANS simulation, with three different FA location for the junk emission and an one second impulse production. Each FA junk is however monitored separately, at four locations: mid HX level, right PP, left PP and core bottom. The initial location of the junk emission event proves to be of great importance to characterize its further short time description. We can also see that it takes about 30 s for the event to propagate up to some HX and about 50 s to propagate back to the core.

To get a closer insight on the LBE level of stagnation in the cold plenum annulus, we have set there a passive scalar, named Decay, with initial unit value and have a look at its evolution after 60 s. The result is shown on Figure 5 where the domain represented is the union of the initial domain with unit value and the current domain with value above 0.9. We can see some defects from the top due to an erroneous dispersion in the cover gas. We can also see a non-negligible evolution at the bottom which can lead in time to a certain renewing of the LBE in this region, confirming the substance of the frozen field calculation.

CONTROL ROD DYNAMICS IN COMPLOT FACILITY

The COMPLOT facility will be an isothermal loop, operating at temperature range of $200°C - 400°C$ with upwards LBE flow. It will be used to test the components pressure drop characteristics and the dynamics of moving parts in LBE. SCK•CEN have conceptualized a test section design where the lower part of the guide tube is inserted into a hexagonal ”pipe” representing the core region. Above the core region, the test section expands into a larger annular flow area which receives the LBE flowing out from the guide tube outlet holes.

Our aim is to numerically reproduce the control rod system in COMPLOT with imposed displacement history (taking into account acceleration and inertial effects), to measure the numerical forces applied to the control rod and to validate them against the experimental tests.

Computational domain

The simulations are performed with the commercial CFD Star-ccm+ code. The construction of the geometrical model started from an existing model, that we have previously realized for the Safety Rod assembly. In the report [5] we realized an optimization parametric study in order to help the designer to choose for the specific dimensions of test section outlet. The geometry of the computational domain is formed by a guide tube filled with LBE which hosts the moving absorber pins bundle. The guide tube expands into a larger annular tube with outlet function. The moving absorber pins bundle is roller guided and is mechanically linked with a central rod that links to a hollow tube long all way throughout the guide tube. The flow path inside the guide tube is formed by a damper, a bypass and a labyrinth flowing out the LBE through a series of outlet holes. In our model, we considered a half of the geometry, by taking advantage of the axial symmetry. We constructed from scratch the CR hosting section, adapting the previously realized one, then we imported the CAD model with the flow paths and the moving components. With boolean operations the different solid components were merged and subtracted from the full guide tube in order to obtain only the fluid domain. The mesh was generated using the polyhedral and the prism layer model, it was refined at boundary level and volumetric controls have been employed in order to better capture some details, obtaining about 3 millions of volume cells.

Movement settings. Strategy of re-meshing

The method for reproducing the movement of the control rod consists in the following: the computational domain is divided in four regions, one containing the moving part, two regions upward and downward, appropriately coupled with the moving

part through interfaces and the fourth one containing the rest of the domain. The movement couples a rigid body motion (translation) of the absorber pins bundle region with a morphing motion of the up and down regions, letting stationary the rest of the domain. The morphing produces deformations of the mesh (in our case, compression and stretching of the volume cells in the up and down regions). In order to control the degeneration of the mesh, we developed some re-meshing strategies, described in detail in the report [6], that we apply in COMPLOT in a selective manner, only on the affected parts. This represents an important achievement since we can save from re-meshing the assembly of the pins, which is the most costly in terms of computational power. The strategy of re-meshing consists in coupling the physical displacement performed by the control rod with the update of the underlying geometry. We retrieve the effective displacement performed by the rod and impose it as translation vector of the corresponding geometrical body at CAD level. At the same time, we control the quality of the mesh by means of appropriate metrics.

As design parameters controlling the variation of the geometry parts we adopted the extrusion distances used in the construction of the guide tube and the vector translation of the bundle. The cylindrical bodies are usually constructed starting from circles that are then extruded with a given length. In the 3D-CAD modeller included in Star-ccm+, the directions of extrusion are quite flexible, so we could choose the asymmetric extrusion of the circular sketch. If the initial extrusion distances (symmetric and asymmetric) of a cylindrical body are d_0, d_0', then the extrusion distances controlling the updating process will be: $d = d_0 + \delta s$ and $d' = d_0' - \delta s$, where δs indicates the effective displacement. The automatic implementation of this strategy is coupled with the simulation through a Java script, according to the following algorithm:

1. Run the simulation for one time step.
2. Control the condition about the mesh quality criterion.
3. If criterion is satisfied, go one time step forward; otherwise:
4. Regenerate the volume mesh, including:
   (a) read the effective displacement performed by the moving part and put it into variables;
   (b) assign the value of d, d', δs to the CAD design parameters (i.e. to the symmetric, respectively the asymmetric extrusion distances, and to the Translation vector);
   (c) re-generate the surface and volume meshes, taking the most recent boundaries as starting point (i.e. the geometry with the updated bundle and with the updated central region position).

Physical settings. Choice of required boundary conditions

We reproduced the CR mechanical movement with the strategy described above, imposing a velocity to the bundle with a given acceleration. This was done by assigning a translation velocity law to the region containing the bundle. The same velocity was set as boundary condition in the regions undergoing the morphing motion, namely, assigning a Grid Velocity to the interfaces with the central region. The other boundaries of the morphed regions have a Floating boundary condition. This means that the points on these boundaries are free to follow the motion of the interfaces.

In order to verify the independence of the solution from the mesh and re-meshing operations, we prepared reports and monitors from which we obtained plots during the simulation. Indeed, the plots of the various physical fields that we monitored show that only small perturbations were noticed, without important effects on the flow, when the mesh had to be regenerated.

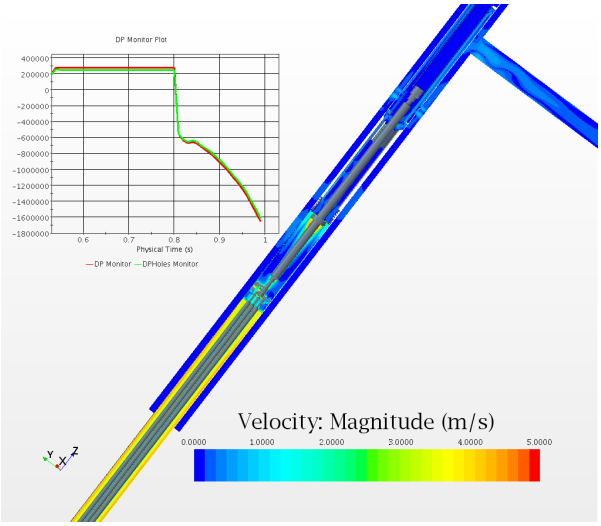

Figure 6. Pressure drop evolution (steady in stationary case, followed by inversion in transient case)

The settings of the simulation were the following ones. We started with a stationary simulation, with a prescribed mass flow rate in inlet and a pressure outlet as boundary conditions. We obtained a fully developed flow in steady state. We also set a different boundary condition, namely a stagnation pressure in inlet. Hence we imposed in inlet the pressure drop between the inlet of the guide tube and the lateral outlet of the annulus. We retrieved the expected mass flow rate in inlet. In the stationary case both approaches proved to be coherent, as expected.

Transient with inlet mass flow rate (MFR)

We continued to run the same simulation switching to transient case, with a time step of 0.01 s. We first kept the bundle stationary for 0.5 s physical time, in order to stabilize the flow; indeed the pressure drop plots were stable at the end of these iterations. After that we let the bundle move, with the velocity $V = 15(Time - 0.5s)m/s$, hence considering the acceleration $a = 15m/s^2$ and leaving out the time in which the bundle was stationary. Due to the complexity of the pins bundle and of the flow path, the objective in this stage of the work was to manage to perform only the first part of the movement, i.e. about a half of the total displacement. We applied several re-meshings during the movement, but with our strategy we managed to avoid the re-meshing of the region containing the pins bundle, that is good news since the bundle alone contains about 2.5 M Cells. The displacement was performed in about 0.2 s, until the seal attached to the rod reaches the entrance in the damper.

During the movement, the simulation revealed a strong depression. The pressure drops presented a sudden variation, reaching a $\Delta P = -6bar$ in the first time step, and continued to get down negative, as shown in Figure 6. In order to figure out whether this strong depression was due to numerical errors or to the imposed acceleration, we run with a smaller (0.001 s) time step and obtained the same pressure evolution. In fact, the pressure inversion was perfectly physical. It was the effect of the enhanced added mass due to the prescribed mass flow rate in inlet and to the strong instantaneous acceleration.

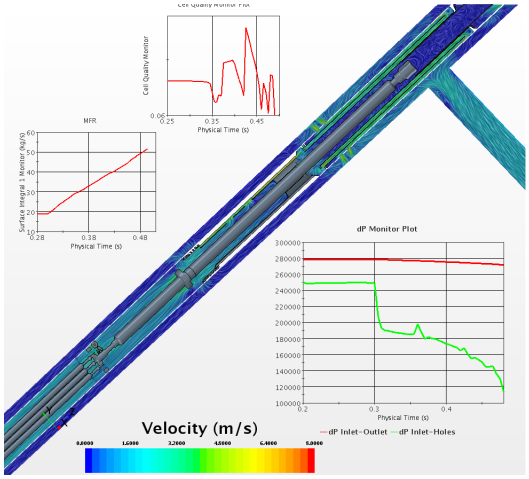

Figure 7. Pressure drop across CR in Complot in presence of re-meshing

Transient with inlet pressure

It was clear from the previous approach that a MFR boundary condition was not compatible with the imposed motion. Hence we adopted a different strategy: initially, we performed the unsteady simulation with the stationary bundle, with given MFR and we calculated the Inlet-Outlet pressure drop. Then we imposed this pressure drop in inlet (Stagnation Inlet BC) and let the bundle to move. Besides the pressure drop across the test section, we also measured the pressure drop across the control rod bundle. The Inlet-Outlet ΔP remained almost constant while the ΔP across the CR bundle (Inlet-Outlet holes) registered a minor jump of $\Delta P = 0.5$ bar in the first iteration and continued to decrease of about 1 bar during the movement. At the same time, we monitored the mass flow rate in inlet during the motion and registered an increasing (tripled) MFR in inlet, confirming the added mass effect. Several automatic re-meshings were applied in base of a cells quality metric. Their effect on the physics is minor (the small jumps in the pressure plot in Figure 7 correspond to the re-meshing operations) and can be however still improved in the future. The situation described here can be contemplated in Figure 7.

LIQUID LEAD SPALLATION TARGET MODEL

In the framework of the THINS project we realized the porting on GPU architecture of the SPH code [7]. The improved technology is applied to the simulation of a liquid metal free surface target that was recently proposed for the European Spallation Source (ESS) project. The results of free surface stability analysis in relatively long times are illustrated as well as the quick transient phenomena and the pressure waves due to the beam power deposition.

The method

The idea at the basis of the method is to approximate any function $f(\mathbf{x})$ of the domain Ω as:

$$f(\mathbf{x}) = \int_{\Omega} f(\mathbf{x}')W(\mathbf{x}-\mathbf{x}',h)d\Omega \qquad (2)$$

The kernel function W is a smooth and differentiable function of the inter-particle distance and of a characteristic or *smoothing length* h. It has a compact support and approximates the Dirac function as h approaches zero, so that it has a unit integral over the domain.

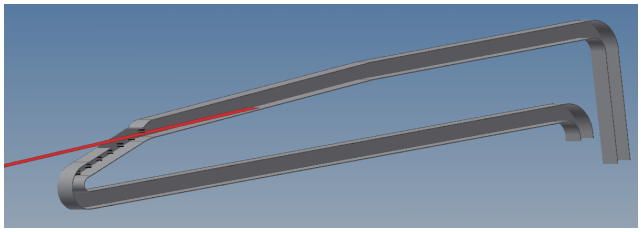

Figure 8. KIT free surface target design for the ESS spallation source

The fluid is discretized as a finite set of particles $i = 1 \ldots n_p$ of given mass m_i, position x_i, velocity v_i, density ρ_i, internal energy density u_i and with known material properties. The value of any field function on the particle is approximated as a discrete sum approximating an integral. In discrete notation, we get the following expression of the value of a function at the particle i position $f_i = \hat{f}(\mathbf{x}_i)$:

$$f_i = \sum_j m_j \frac{f_j}{\rho_j} W_{ij} \qquad (3)$$

where $W_{ij} = W(\mathbf{x}-\mathbf{x}',h)$ and the sum is carried out on all the particles, m_j and ρ_j are the "j" particle mass and density, their ratio is the portion of volume occupied by a particle. Therefore the value of a field function is calculated as an integral mean, evaluated numerically on the position of the particles around the point of interest. The method is used to approximate the Euler equations. It may be applied to gases, liquid and solids, the appropriate Equation Of State (EOS) closes the system and gives the value of the particle pressure as a function of density and internal energy.

Free surface target for ESS

The accelerated version of the SPH code was applied to the analysis of a liquid metal target, to test the potential of the code and to define and verify the simulation techniques that may be adopted. The example described may be used as a reference for similar analysis with different geometries, materials and boundary conditions. We used as a reference the free surface concept for the European Spallation Source, recently developed by KIT shown in Figure 8.

The European Spallation Source ESS aims at producing high energy spallation neutrons. They are produced when a high energy ($W = 2500MeV$) proton beam with a mean current of $I = 2mA$ hits an appropriate target material. Inherently coupled to the desired spallation reaction is the high heat deposition in the target. This power is mainly due to the proton current and can be calculated as the product of the energy of a single proton times the number of protons per second in the beam, i.e. $Q = UI = 5MW$.

In ESS the high beam power is provided by a pulsed source with a repetition rate of $f = 20Hz$. The duration of the pulses is "long" for this kind of application and is chosen equal to $1ms$. With each pulse the target material is heated by the proton beam, the amount of energy deposed in the target as heat source may be estimated through neutronics calculations and in this case amounts to $2.3MW$. The heating is non-uniform, as the heat

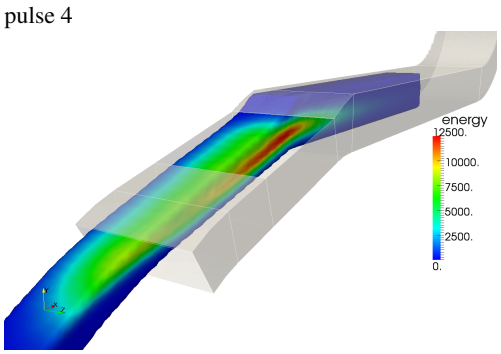

Figure 9. Target heating, a cutoff of the model is shown for clarity. The specific energy of $12.5kJ/kg$ causes a temperature rise of $85K$

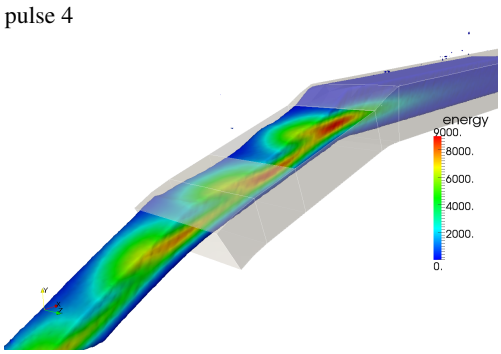

Figure 10. Target heating with double mass flow rate. The specific energy of $9kJ/kg$ causes a temperature rise of $62K$

deposition strongly varies in the material; heating is accompanied with thermal expansion of the target material and thus with thermal stresses and potentially with pressure waves.

In a windowless target the material is a liquid metal which is pumped through a cooling loop to remove the heat. The proton beam is directed on a free surface, so that no solid structures are subjected to the proton beam. The target module is installed at the exit of the heat exchanger. The flow is pumped upwards, then directed into a horizontal channel and then accelerated by a nozzle into an open channel. Following each pulse, a complex shock wave is generated in the channel. We expect a pressure peak propagating in the pipes and potentially damaging the nozzle itself and the rest of the equipment. Moreover since a free surface is directly exposed to the proton beam deposition, a splashing phenomenon may take place, and the liquid material of the target may be ejected through the window.

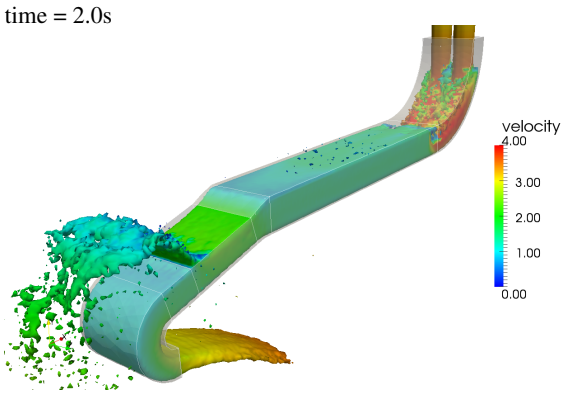

Figure 11. Particle velocity in the target when an elbow with an high curvature is adopted at the outlet

Target filling and beam heating

In order to run the heating transient simulation we need first to obtain a steady state condition with a free surface. The easiest way to obtain this is to simulate a fill up of the channel, from the empty condition to a steady state regime. The inlet boundary introduces LBE particles with the target rate and the pump gives the liquid the desired value of velocity.

The simulation starts from a fully developed flow, to which we apply the beam power deposition in pulses of $1ms$ duration with a frequency of $20Hz$. The Figure 9 shows the energy distribution inside the model after the impact of the first four pulses.

It is clear that the energy and temperature distribution is soon regularized, and presents a maximum along the beam axis at the beginning of the inlet channel.

The maximum energy density is higher than that due to a single pulse, it is actually almost double: this is due to the superposition of subsequent pulses. In order to reduce the maximum energy it is anyway possible to increase the fluid velocity, as long as this does not have effects on the free surface stability.

The peak energy density in the model is calculated in $12.5kJ/kg$, corresponding to a temperature increase of $85K$ given a specific heat of $146J/kgK$.

The results for a double mass flow rate are shown in Figure 10. It is clear that in this condition the superposition of subsequent pulses is much lower and therefore the maximum energy and temperature increase in the LBE is lower than the one obtained in the design conditions.

The outlet conditions may play an important role in the stability of the free surface in the window area. It was evident that increasing the velocity causes the fluid to have a point of contact progressively closer to the window. The use of an elbow to close the liquid metal circuit has to be carefully evaluated and its shape has to be designed properly. We checked a model in which the channel duct forms an elbow with a very short curvature radius. The filling up simulation clearly shows that this cannot be a good solution. Too much counter pressure is generated at the exit and the liquid metal is actually ejected through the window as shown in Figure 11.

Pulse transient

Due to Joule heating by the proton beam, the temperature of the LBE rises locally during the pulse. The heating induces a thermal expansion. The thermal expansion pushes the surrounding fluid radially outward, so that a pressure peak forms along the proton beam axis.

At the end of the pulse, the fluid is still moving outwards while the thermal expansion has come to an end, resulting in tensile stresses on the central area of beam deposition. Therefore, first a compressive and then a tensile shock wave are generated. Whereas the liquid is supposed to withstand any value of positive pressure, if negative pressure is lower than a certain limit cavitation may take place, and the continuity of the liquid is broken by the formation or the growth of gas bubbles.

The liquid metal is subject to a complex pattern of shock waves due to the thermal expansion. It appears that the most intense pressure waves are generated at the beginning and at

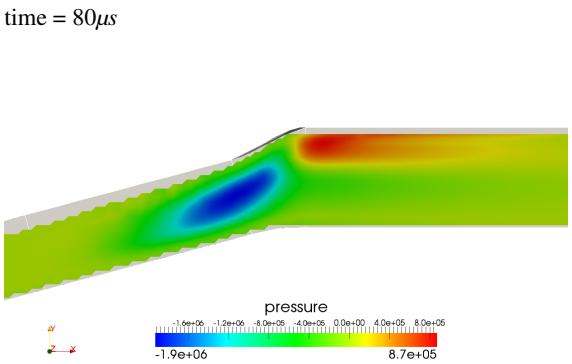

Figure 12. Pressure distribution [Pa] in the symmetry plane of the target when a material without tensile limit is considered

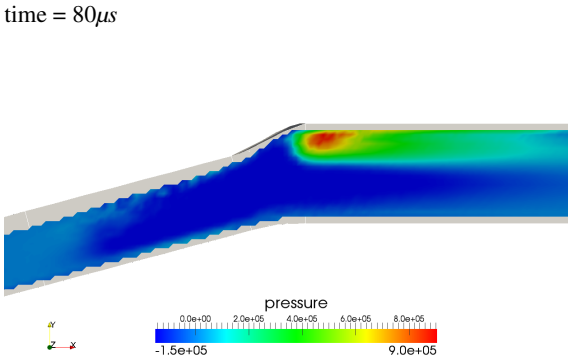

Figure 13. Pressure distribution [Pa] in the symmetry plane of the target when a material without a tensile limit of $150kPa$ is considered

the end of each pressure pulse. The multiple reflection of these waves inside the channel soon lead to a difficulty in the interpretation of the pressure pattern. Figure 12 shows the pressure distribution in the vertical plane containing the beam axis at the very beginning of the beam deposition. In this analysis, we did not use the tensile limit for the material.

The pressure distribution in the plane is characterized by an oscillation of positive and negative pressure areas that remain concentrated around the beam deposition and that does not seem to propagate significantly along the channel. The presence of a free surface in fact has the effect of reducing the pressure peaks in the circuit.

The same analysis was run with a limit of $150kPa$ on the negative pressure and the results are shown in Figure 13. The pattern is similar but the material limits the tensile value and rapidly dissipates the mechanical energy.

The pressure peak in both model is quite high inside the liquid, it is in fact well above $20bar$. It is anyway interesting to notice that the pressure on the contact surface is much lower. This is due to the fact that the containing structure has a limited rigidity, and this greatly reduces the pressure on it and the consequent stresses.

We run the simulation for a longer time to verify whereas any splashing phenomenon may take place in the design condition. In a total time of $100ms$ corresponding to two beam pulses no splashing phenomenon takes place, and only a small deformation of the free surface is barely visible.

In order to verify the limits of the target design, we tried to

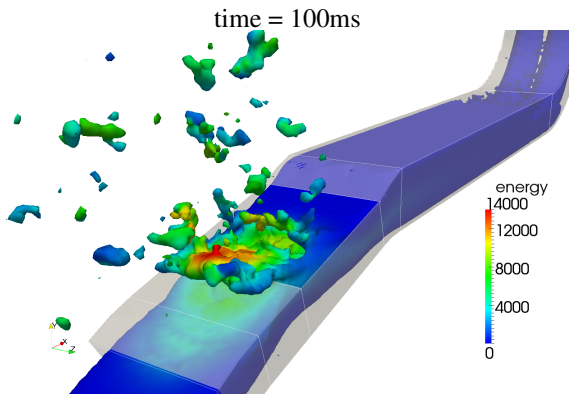

Figure 14. Transient response to the pulsed heating for a pulse length of $10\mu s$. The energy density is in $[J/kg]$.

modify the design conditions and see what may be the consequences of the adoption of a shorter pulse. All the boundary conditions of the problem are left unchanged with the only exception of the beam pulse, that is now 100 times shorter and 100 times more powerful, to keep unchanged the total deposited energy per pulse, the pulse length is now $10\mu s$, the frequency is still $20Hz$ and the beam power is $500MW$ due to the higher current considered. The evolution of the free surface is shown in Figure 14. In this case it is evident that something similar to an explosion takes place inside the material. The propagating shock wave is totally converted in kinetic energy when it reaches the free surface and causes a splashing. The use of a tensile limit dissipates part of the mechanical energy but this is not sufficient to avoid the phenomenon.

Conclusions

The model of the MYRRHA primary coolant loop is going toward a full 3D complete simulation combining a free-surface flow and a thermal flow, driven by hydraulic pumps. The heat provided by the reacting nuclear core is removed by the heat exchangers. The developed model is ready for use and will serve for the analysis of the buoyant passive scalars and Lagrangian particles dispersion, as well as for the simulation of partial loss of coolant and pump loss.

The CFD simulation of the MYRRHA control rod dynamics was realized in preliminary transients using moving meshes techniques and automatic optimized re-meshing strategies. Full-scale CFD simulations of the control rod displacement in its guide tube filled with LBE have been set up taking into account the buoyancy as driving force. Suitable boundary conditions compatible with the imposed motions have been found and applied. The further work will focus on the reproduction of the control rod movement in the more complex flow path using overset meshes and sliding interfaces.

The SPH code Armando has been ported on a GPU architecture with good results in terms of performance acceleration. The code has been applied to a complete analysis of a liquid metal target proposed by KIT for the ESS project. The results show the capability of the code to model all the significant transients of a free surface liquid, and verify the free surface stability, the filling up of the channel, the energy distribution inside the metal at different flow rates, the influence of the channel geometry on the flow configuration and most important, the fast transients and pressure waves generated by a pulsed beam deposition. The developed application may be a valuable tool for the design and

analysis of liquids with free surface and subject to fast heating.

NOMENCLATURE

C_p	isobaric specific heat $[J/Kg/K]$
R	hydraulic resistance $[Kg/m^2s^2]$
v	velocity $[m/s]$
ρ	density $[kg/m^3]$
τ	characteristic time $[s]$

REFERENCES

[1] Official website www.myrrha.sckcen.be

[2] Official website www.cd-adapco.com

[3] V. Moreau, Towards a full 3D simulation of MYRRHA primary coolant loop, *Lecture Series: Fluid Mechanics and Chemistry for Safety issues in HLM nuclear reactors*, Von Karman Institute, 2013, Belgium

[4] *Handbook on Lead-bismuth Eutectic Alloy and Lead Properties, Materials Compatibility, Thermal-hydraulics and Technologies, 2007 Edition* OECD/NEA Nuclear Science Committee, OECD 2007, NEA No. 6195

[5] M. M. Profir, V. Moreau, G. Kennedy, CFD Optimization of the COMPLOT Test Section Outlet, CRS4 Technical Report, October 25, 2012

[6] M.M. Profir, Automated moving mesh techniques and re-meshing strategies in CFD applications using morphing and rigid motions, CRS4 Technical Report, http://publications.crs4.it/pubdocs/2012/Pro12c.

[7] L. Massidda, Transient simulation of a windowless spallation target with Armando, THINS project report, Deliverable D4.2.06, CRS4, 2013